

CrossMark
click for updates

Article submitted to journal

Subject Areas:

astrophysics, stars, spectroscopy

Keywords:Solar corona, elemental abundances,
solar flares, solar-stellar connection**Author for correspondence:**

David H. Brooks

e-mail: dhbrooks.work@gmail.comDynamic modeling of coronal
abundances during flares on
M-dwarf starsDavid H. Brooks^{1,2}, Jeffrey W. Reep³,
Andy S.H. To⁴, Luke Fushimi Benavitz⁵
and Lucas A. Tarr⁶¹Computational Physics, Inc., Springfield, VA 22151,
USA²University College London, Mullard Space Science
Laboratory, Holmbury St. Mary, Dorking, Surrey, RH5
6NT, UK³Institute for Astronomy, University of Hawai'i,
Pukalani, HI 96768, USA⁴ESTEC, European Space Agency, Keplerlaan 1, PO
Box 299, NL-2200 AG Noordwijk, Netherlands⁵Institute for Astronomy, University of Hawai'i,
Honolulu, HI 96822, USA⁶National Solar Observatory, 22 Ohi'a Ku St.,
Makawao, HI 96768, USA

Solar atmospheric elemental abundances are now known to vary both in space and time. Dynamic modeling of these changes is therefore necessary to improve the accuracy of radiative hydrodynamic simulations. Recent studies have shown that including spatio-temporal variations in coronal abundances during solar flares leads to the formation of coronal condensations (rain), which are otherwise difficult to create in impulsively heated field aligned hydrodynamic flare models. These simulations start with a solar corona dominated by the first ionization potential (FIP) effect, and evaporate photospheric material into the post-flare loops. We here explore perhaps the most extreme non-solar starting condition for the coronal composition in these simulations: an initial corona dominated by the inverse FIP (iFIP) effect, such as is observed on active M-dwarf stars. We show that a flaring event in a corona enriched with high FIP elements leads to a solution similar to the solar case. Coronal rain is harder to form by this method during flares on M-dwarfs, however, if the corona is depleted of low FIP elements.

© The Authors. Published by the Royal Society under the terms of the Creative Commons Attribution License <http://creativecommons.org/licenses/by/4.0/>, which permits unrestricted use, provided the original author and source are credited.

1. Introduction

The solar corona is sustained by mass and energy flow from the lower atmospheric layers, so the elemental composition was originally expected to be the same as that of the photosphere. Analysis of UV spectra, however, showed that the abundances of Fe, Si, and Mg, are closer to the values seen in planetary nebulae and cosmic rays [1]. In fact, the slow solar wind also shows what is now known as the FIP (First Ionization Potential) effect [2] i.e. a relative overabundance by a factor of 2-3 compared to the photosphere, of elements with a low FIP (less than ~ 10 eV). Recent observations from the *Hinode* EUV Imaging Spectrometer (EIS) [3] have also highlighted that plasma composition can vary significantly both spatially and temporally in many coronal features. See, for example, composition measurements over the full solar disk [4,5], in locations in post-flare loops where coronal rain becomes noticeable [6], or unusual X-shaped flare ribbons [7] and current sheets [8], and even the detection of the inverse FIP (iFIP) effect - the depletion of low FIP elements or enhancement of those with a high FIP (>10 eV) - in localized regions of sunspots during solar flares [9].

Similar abundance variations are seen in spatially unresolved observations of solar-like stellar coronae. A previous study reported a strong correlation between the observed FIP effect and the stellar spectral type [10]. That is, there is a progression from a solar-like FIP effect in G-type stars, through a smaller (or no) effect in K-type stars, to a strong iFIP effect in M-dwarfs. There may also be variations with the activity cycle, as observed on the Sun-as-a-star [11]. For further discussion, see also the review in this issue [12] for references on changes over widely variant timescales from months (active regions) to years (solar cycle).

Large enhancements and spatio-temporal variations in element abundances make a significant difference to the radiative cooling properties of the coronal plasma [13], and therefore can potentially impact numerical modelling and comparisons with observations. This is because increases (or decreases) in elemental abundances, regardless of ionisation potential, lead to stronger (or weaker) radiation from spectral lines emitted by ions of those species, which in turn results in a greater (or lesser) contribution to the total radiative losses. If the magnitude of the radiative losses is larger (or smaller) this leads to faster (or slower) cooling.

There have been some recent advances made in studying these impacts. To investigate the inverse FIP (iFIP) effect in solar flares, different radiative loss functions reflecting the enhancement/depletion of high/low FIP elements were added as look-up tables to the (Enthalpy Based Thermal Evolution of Loops) EBTEL [14,15] 0-D hydrodynamic code [16], and analysis of the resultant post-flare loop cooling times showed that the low FIP elements were likely depleted. A similar simulation setup was used to match simulated loop cooling times with the observed cooling times of different locations in a post-flare loop arcade with known (measured) abundances [17]. In both these cases, the starting (static) radiative loss function was altered to look for diagnostic differences in the cooling times, but the studies were not based on a physical model for the abundance changes.

The EBTEL++ code [18,19] has now been updated to incorporate time-variable abundances as a weighted average between the initial assumed coronal value and the material carried into the corona via chromospheric evaporation [20]. More recently, the 1-D HYDroynamics and RADiation (HYDRAD) code [21,22] has been modified to include an abundance factor that is variable in both space and time [23]. The study also looked at the formation of coronal rain.

Coronal rain has been observed in UV/EUV data since at least the 1970s (see e.g. [24], and references therein), but was only studied occasionally [25,26]. In recent years its importance has become more widely recognised and it has become intensively studied observationally [27–31]. Coronal rain is thought to consist of cool, dense plasma condensations that form due to a thermal instability when coronal loops cool catastrophically [32]. It appears in 3-D radiative MHD simulations when the thermal instability is triggered by chromospheric evaporation in response to heating associated with magnetic field line braiding [33]. It can also be produced in 1-D hydrodynamic simulations if the heating is localized to the loop footpoints. In fact there

are several avenues to producing these instabilities including the effects of flows and magnetic topology. See [34] for a recent comprehensive review.

One outstanding issue is that it is difficult to produce coronal rain in electron beam heating simulations of flare loops that assume a constant, or monotonically decreasing, magnetic field strength with height [35]. [23] performed two loop simulations of typical short-duration impulsive heating (nanoflares) and strong electron beam heating (flares) in active region loops. They found that including spatio-temporally varying abundances causes coronal loop condensations (coronal rain) to form at the loop apex due to a localized peak in the radiative losses relative to other values along the loop. This peak results from the localized enhancement in low FIP elements that forms because material evaporating from the chromosphere pushes the coronal plasma to the apex.

Future work will determine the range of parameters necessary to produce coronal rain in typical solar flare conditions. An interesting question that arose during discussions of this work at the Theo Murphy meeting was whether we could formulate an extreme test of this simulation in quite different conditions from the solar case? In Sun-as-a-star time-series observations of solar flares, the initial coronal abundance moves towards photospheric values due to chromospheric evaporation [36,37]. Similar behaviour is commonly seen in flares on solar analog stars, and in fact the basic picture of evaporation of photospheric composition plasma into the corona seems to hold regardless of the initial coronal composition since it has also been seen on some stars with iFIP coronae in their quiescent state [38]. The latter would certainly represent a very different scenario from the solar case since the Sun and M-dwarfs sit at opposite extreme ends of the spectral type versus FIP effect correlation [10]. To give some specific examples, increases from ~ 0.3 and $\sim 0.6\times$ solar photospheric to ~ 1 and $\sim 1.4\times$ photospheric were measured during flares observed on the eclipsing binary Algol using metals and the M6 variable star CN Leo (Wolf 359) using Fe [39,40]. Increases in Fe and Si abundances from values below those of the solar photosphere were also observed during a flare on the RS CVn binary HR 1099 using XMM-Newton [41], and this has been seen again very recently, for Fe and Ca during a flare, in HR 1099 observations from the Resolve instrument on XRISM [42].

Here we model the response of an iFIP corona in an M-dwarf star, to strong electron beam heating of the stellar chromosphere during a flare. Based on measurements of coronal abundances as a function of stellar spectral type, the simulations are broadly applicable to the coronae we expect in M-dwarf stars [10,43]. Since our goal here is to assess the impact of adopting an iFIP corona as the starting condition, we decided to control the experiment by closely matching the rest of the model parameters from [23], and simulating a moderate solar flare. Flares of this magnitude should occur more frequently on M-dwarfs, but the distribution of flare energies spans a much larger range than on the Sun [44]. Our simulation therefore likely represents a flare from the cooler end of the M-dwarf distribution. We simulate two iFIP scenarios: 1) the enrichment of high FIP (>10 eV) elements in the corona, and 2) the depletion of low FIP elements in the corona. Although these two possibilities exist in active stars, evidence from theoretical modeling [45–47], observations of solar post-flare loop cooling times [16] and column depths [48], and the detection of the iFIP effect in the slow solar wind [49], all suggest that the FIP effect operates to deplete low FIP elements, so this may be the more likely scenario.

2. Loop simulations

We use HYDRAD for our calculations, including optically thick chromospheric radiation [50] and optically thin radiative losses computed using the CHIANTI database v.10 [51,52], assuming ionisation equilibrium within HYDRAD for the 15 most abundant elements. We also adopt the photospheric abundances of [53]. HYDRAD is open source and is publically available¹. The flare simulation setup follows the electron beam heated case of [23] with two modifications. In general, coronal loop lengths are significantly larger on M-dwarfs [54], so we adopt a loop length of 150 Mm. The other modification is a reduced heating duration. We initiate the electron beam at the

¹<https://github.com/rice-solar-physics/HYDRAD>

start of the simulation with a constant flux of 2×10^{10} erg cm⁻² s⁻¹ for 10 s, a cutoff energy of 15 keV, and a spectral index of 5. Adaptive mesh refinement is employed to ensure adequate spatial resolution in the transition region, with each grid cell allowed to split up to 12 times.

Our treatment of spatial and temporal abundance changes also uses the HYDRAD implementation of [23]. This implementation is also publically available² and modifications specific to this work have been placed in a Zenodo archive [55]. The radiative loss rate within the simulation is modified by an abundance factor $f(t, s)$ that is variable in space, s , and time, t . f evolves due to flows along the loop following the advection equation

$$\frac{\partial f}{\partial t} + v \frac{\partial f}{\partial s} = 0. \quad (2.1)$$

where v is the bulk flow velocity. In what follows, we add a subscript H or L to be clear whether high or low FIP elements are being modified.

We perform two simulations of a flare occurring in an iFIP dominated stellar corona. As discussed in the introduction, solar observations [16,48,49] and models [45–47] currently favor the idea that low FIP elements are depleted in the solar iFIP effect, but even if correct this may not be the case in very different stellar coronae. We therefore explore two possible scenarios. For the first simulation we assume the corona is initially enriched with high FIP elements by a factor of 4 and define $f_H = 4$ in the corona. In our second simulation we assume that the low FIP elements are depleted and set $f_L = 0.25$ in the corona. In both cases we set $f = 1$ (photospheric abundances) in the chromosphere. Both initial conditions were implemented with a step function between the photospheric and coronal values at a distance of 2.26 Mm (the base of the transition region) from both ends of the loop.

3. Results

The results of our simulation starting from a corona enriched with high FIP elements is shown in Figure 1. Due to the broadly similar temperature coverage of low and high FIP elements, the enhancement of high FIP elements to a factor of $f_H = 4$ results in a radiative loss function that is expected to be broadly similar to the one that would be obtained if the low FIP elements were enhanced instead. This is indirectly confirmed in Figure 1 where the results are similar to the solar case presented by [23].

Broadly speaking, impulsive heating simulations produce a loop that heats up uniformly and then cools down [35]. The overall cooling time of the loop is dictated by the cooling timescales of radiation, conduction, and enthalpy fluxes [56–59]. The radiative cooling timescale depends on the ratio of thermal energy ($\propto n$) to the radiative loss rate ($\propto n^2$) and is therefore affected by both the density ($\propto 1/n$) and the abundances that dictate the slope of the radiative loss curve, which dominates the cooling after the density peaks following evaporation.

In our simulation, once chromospheric evaporation in response to the electron beam heating begins, material flows into the loop from the photospheric footpoints. The abundance factor then starts to decrease rapidly along the loop. This pushes plasma towards the loop top to produce a localized peak in high FIP element abundances (factor f_H) and an associated spike in the radiative losses. Although the loop has initially heated up in a uniform manner, the localized peak in radiative losses causes enhanced cooling at the loop apex leading to a local decrease in pressure and the formation of a pressure gradient that feeds the region with plasma and raises the density at the apex. This then exacerbates the runaway radiative cooling and forms a coronal condensation. One consequence of the longer loop length in the simulation is that chromospheric evaporation takes longer to fill the loop and the condensation forms later than in [23]. They found that the condensations formed after ~ 2000 s, whereas here it takes more than 5000 s. The condensation is also not located exactly at the apex. The result, however, confirms that an iFIP corona enriched with high FIP elements can lead to the formation of coronal rain during stellar flares.

²<https://github.com/jwreep/HYDRAD/tree/Abundances>

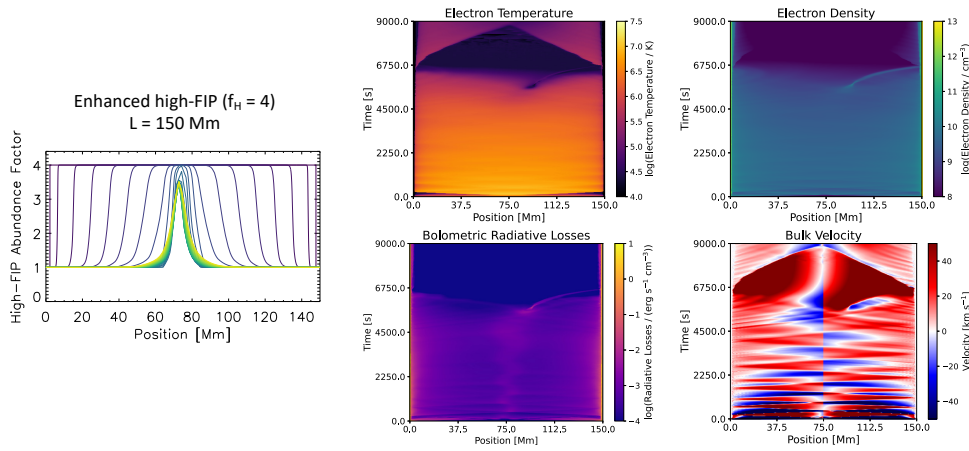


Figure 1. Electron beam heated loop simulation for the case where high FIP elements are enhanced in the initial corona. Left panel: abundance factor as a function of position along the loop. Time is coded by color (purple→green→yellow) in 10 s increments for the first 500 s of the simulation i.e. approximately the initial 17% of the total simulation time shown in the subsequent panels. Middle panel: electron temperature (top) and bolometric radiative losses (bottom) as a function of time along the loop. Right panel: electron density (top) and bulk flow velocity (bottom) as a function of time along the loop. Red/blue velocities indicate flows away from/towards the loop apex. The corona is initially enriched with high FIP elements by a factor of 4 (iFIP effect), but the abundances decrease rapidly towards photospheric values ($f_H=1.0$) due to chromospheric evaporation as the loop heats up. This is similar to the simulation shown in [23]. A localized peak in f_H forms at the loop apex, which produces an associated increase in radiative losses and a faster cooling time. A coronal rain condensation forms.

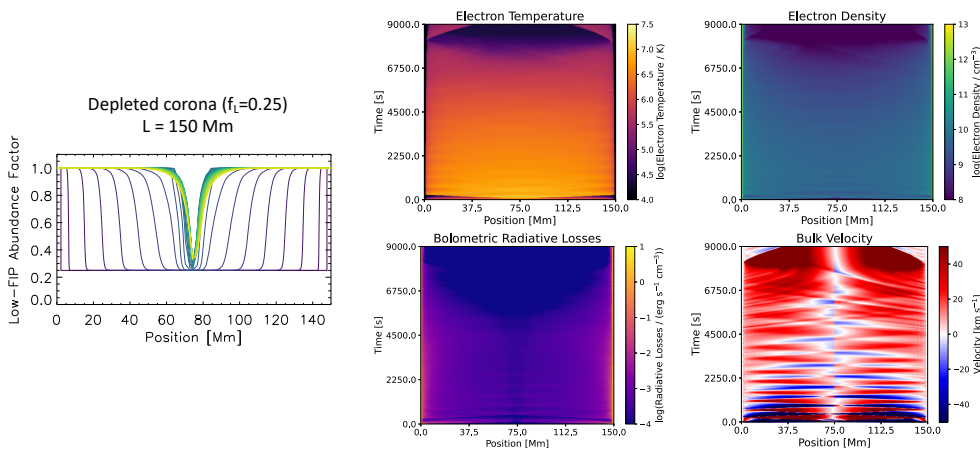


Figure 2. Same as Figure 1 but for the case where low FIP elements are depleted in the initial corona. The corona is initially depleted of low FIP elements by a factor of 4 (iFIP effect), but the abundances increase rapidly towards photospheric values ($f_L=1.0$) due to chromospheric evaporation as the loop heats up. This is opposite to the simulation shown in Figure 1 and in [23]. A localized dip in f_L forms at the loop apex, which produces an associated decrease in radiative losses and a longer cooling time. No coronal rain condensation forms.

The results of our simulation starting from a corona depleted of low FIP elements are shown in Figure 2. In this case, the depletion factor of $f_L = 0.25$ produces a radiative loss function that has

a smaller magnitude than the solar photospheric one. See Figure 1 of [16] for an example. As can be seen in Figure 2, photospheric material flows into the loop due to chromospheric evaporation, and causes a rapid increase in the abundance factor along the loop. As in the previous simulation, an accumulation of material with the initial coronal abundances forms at the loop top. This time, a localized dip in abundances of low FIP elements (factor f_L) is produced with an associated reduction in the radiative losses. The localized decrease in radiative losses causes reduced cooling at the loop apex, so the loop effectively heats up and cools down in a uniform manner without any formation of a condensation, as in simulations with fixed radiative losses [35]. Coronal rain is therefore difficult to form by this method in an iFIP corona depleted of low FIP elements, at least for these model conditions.

4. Discussion

Measurements of elemental abundances in the solar upper atmosphere have revealed several important issues. Plasma composition varies spatially between different regions and features, and also varies as a function of time. Such variations modify theoretical radiative loss functions, and this in turn affects the cooling rate of the coronal plasma. Elemental abundance changes should therefore be incorporated into radiative hydrodynamic and magnetohydrodynamic models for future studies.

Previous work has highlighted the impact of including spatio-temporally varying abundances in simulations of electron beam heating in flares [23]. It was shown that the evaporation of chromospheric plasma into post-flare loops leads to a localized peak in the radiative loss rate that allows coronal condensations to form. This has been difficult to produce in previous field aligned hydrodynamic simulations of electron beam heating in flare loops that assume a constant magnetic field strength with height.

Here we have performed two simulations to further demonstrate the impact of elemental abundances that vary in space and time. We set up a quite extreme contrasting example to the previous study that attempts to mimic the coronal composition found on active M-dwarf stars. These stars possess iFIP quiescent coronae, very different from the Sun, but as discussed in the introduction, stellar observations suggest that photospheric material is evaporated during stellar flares.

Observations suggest that the solar iFIP effect is due to the depletion of low FIP elements, but this may not be the case in the very different conditions on M-dwarf stars. An alternative possibility is that the iFIP effect there is due to the increase of high FIP elements. We therefore modeled both scenarios. The enrichment of high FIP elements leads to a result that is similar to the solar case. The depletion of low FIP elements, however, leads to reduced cooling at the loop apex, so the thermal runaway that causes condensations to form does not occur.

Our results suggest that coronal rain is less likely to form due to electron beam heating during flares on M-dwarfs. We should note that there are significant differences on these stars compared to the solar case, however. Our simulations take into account one aspect of these differences: the expected longer loop lengths [54]. This apparently makes it even harder for chromospheric evaporation to form condensations. Conversely, the heating rates would be expected to be higher and that could potentially cause faster evaporation. One simplification is that our symmetric loop setup is somewhat idealised. In this issue, [60] have shown that asymmetric heating affects whether and where coronal rain can form. In particular, heating that is half as strong in one leg compared to the other leg does not result in rain formation. This is because the localized peak in radiative losses at the apex is dissipated. We have verified this is also true in the longer 150 Mm loop case. If the heating rate is much stronger, however, or the elemental composition at the loop footpoints is also asymmetric, coronal rain can form and it may appear further down the loop leg. This competition between loop length, loop geometry, and heating rate will be further tested in future. Furthermore, our radiation modelling assumes ionization equilibrium, an optically thin corona, and solar photospheric abundances. Relaxing these assumptions is another avenue to

explore. We have included all of our simulations in the Zenodo archive [55] for interested readers (including those not shown here).

Notwithstanding these issues, and the exotic nature of some solar-like stars, we expect that the basic physics of the HYDRAD model is applicable to M-dwarfs. That said, it would be challenging to observationally resolve coronal rain condensations on these stars. It is worthwhile, then, to reflect on what other aspects of these simulations might be detectable in stellar observations. One potential diagnostic is the cooling rate. Despite the fact that both simulations evaporate photospheric material during the impulsive event, the initial cooling function is significantly different. This implies that the cooling behaviour would also be different. Considering the initial cooling functions alone, if high FIP elements are enhanced, we expect a transition from faster to slower cooling, whereas if low FIP elements are depleted, we expect a transition from slower to faster cooling. Of course the modeling is complex. The coronally averaged radiative losses in our two simulations initially track each other quite closely. At later times, when the condensation can form, we see diverging behaviour and multiple changes in which case cools faster or slower at any given time. This behaviour could be detectable in the light curves of different EUV wavelength ranges, or X-ray energy bins, covering spectral lines formed at different temperatures. It has been argued that coronal rain may be seen in optical light curves from the Transiting Exoplanet Survey Satellite (TESS) in the flare late-phase [61]. Also, for X-ray instruments observing energy ranges dominated by Fe emission, for example, we ought to only detect abundance variations if the low FIP elements are depleted. As discussed, snapshots of abundance variations have been detected in high resolution spectra from XRISM [42], and, despite the associated model fit uncertainties, also in time-resolved observations from NICER [62].

Acknowledgements. We thank Miki Kurihara for helpful discussions on stellar X-ray observations. We also thank the Royal Society for its support throughout the organization of the Theo Murphy meeting and the production of this special issue. The work of DHB was performed under contract to the Naval Research Laboratory and was funded by the NASA Hinode program. CHIANTI is a collaborative project involving George Mason University, the University of Michigan (USA), University of Cambridge (UK) and NASA Goddard Space Flight Center (USA).

References

1. Pottasch SR. 1963 The Lower Solar Corona: Interpretation of the Ultraviolet Spectrum.. *apj* **137**, 945. ([10.1086/147569](https://doi.org/10.1086/147569))
2. Meyer JP. 1985 Solar-stellar outer atmospheres and energetic particles, and galactic cosmic rays. *ApJS* **57**, 173–204. ([10.1086/191001](https://doi.org/10.1086/191001))
3. Culhane JL, Harra LK, James AM, Al-Janabi K, Bradley LJ, Chaudry RA, Rees K, Tandy JA, Thomas P, Whillock MCR, Winter B, Doschek GA, Korendyke CM, Brown CM, Myers S, Mariska J, Seely J, Lang J, Kent BJ, Shaughnessy BM, Young PR, Simnett GM, Castelli CM, Mahmoud S, Mapson-Menard H, Probyn BJ, Thomas RJ, Davila J, Dere K, Windt D, Shea J, Hagood R, Moye R, Hara H, Watanabe T, Matsuzaki K, Kosugi T, Hansteen V, Wikstol Ø. 2007 The EUV Imaging Spectrometer for Hinode. *Sol. Phys.* **243**, 19–61. ([10.1007/s01007-007-0293-1](https://doi.org/10.1007/s01007-007-0293-1))
4. Brooks DH, Ugarte-Urra I, Warren HP. 2015 Full-Sun observations for identifying the source of the slow solar wind. *Nature Communications* **6**, 5947. ([10.1038/ncomms6947](https://doi.org/10.1038/ncomms6947))
5. Mihailescu T, Baker D, Green LM, van Driel-Gesztelyi L, Long DM, Brooks DH, To ASH. 2022 What Determines Active Region Coronal Plasma Composition?. *ApJ* **933**, 245. ([10.3847/1538-4357/ac6e40](https://doi.org/10.3847/1538-4357/ac6e40))
6. Brooks DH, Reep JW, Ugarte-Urra I, Unverferth JE, Warren HP. 2024 Spectroscopic Observations of Coronal Rain Formation and Evolution Following an X2 Solar Flare. *ApJ* **962**, 105. ([10.3847/1538-4357/ad18be](https://doi.org/10.3847/1538-4357/ad18be))
7. To ASH, Long DM, Baker D, Brooks DH, van Driel-Gesztelyi L, Laming JM, Valori G. 2021 The Evolution of Plasma Composition during a Solar Flare. *ApJ* **911**, 86. ([10.3847/1538-4357/abe85a](https://doi.org/10.3847/1538-4357/abe85a))
8. Warren HP, Brooks DH, Ugarte-Urra I, Reep JW, Crump NA, Doschek GA. 2018 Spectroscopic

- Observations of Current Sheet Formation and Evolution. *ApJ* **854**, 122. ([10.3847/1538-4357/aaa9b8](https://doi.org/10.3847/1538-4357/aaa9b8))
9. Doschek GA, Warren HP, Feldman U. 2015 Anomalous Relative Ar/Ca Coronal Abundances Observed by the Hinode/EUV Imaging Spectrometer Near Sunspots. *ApJL* **808**, L7. ([10.1088/2041-8205/808/1/L7](https://doi.org/10.1088/2041-8205/808/1/L7))
 10. Wood BE, Linsky JL. 2010 Resolving the ξ Boo Binary with Chandra, and Revealing the Spectral Type Dependence of the Coronal “FIP Effect”. *ApJ* **717**, 1279–1290. ([10.1088/0004-637X/717/2/1279](https://doi.org/10.1088/0004-637X/717/2/1279))
 11. Brooks DH, Baker D, van Driel-Gesztelyi L, Warren HP. 2017 A Solar cycle correlation of coronal element abundances in Sun-as-a-star observations. *Nature Communications* **8**, 183. ([10.1038/s41467-017-00328-7](https://doi.org/10.1038/s41467-017-00328-7))
 12. Brooks DH, Baker D, Long DM, Testa P, Warren HP. 2026 Evolution of Solar and Stellar Coronal Abundances due to Magnetic Activity. *Phil. Trans. A*.
 13. Cook JW, Cheng CC, Jacobs VL, Antiochos SK. 1989 Effect of Coronal Elemental Abundances on the Radiative Loss Function. *ApJ* **338**, 1176. ([10.1086/167268](https://doi.org/10.1086/167268))
 14. Klimchuk JA, Patsourakos S, Cargill PJ. 2008 Highly Efficient Modeling of Dynamic Coronal Loops. *ApJ* **682**, 1351–1362. ([10.1086/589426](https://doi.org/10.1086/589426))
 15. Cargill PJ, Bradshaw SJ, Klimchuk JA. 2012 Enthalpy-based Thermal Evolution of Loops. II. Improvements to the Model. *ApJ* **752**, 161. ([10.1088/0004-637X/752/2/161](https://doi.org/10.1088/0004-637X/752/2/161))
 16. Brooks DH. 2018 A Diagnostic of Coronal Elemental Behavior during the Inverse FIP Effect in Solar Flares. *ApJ* **863**, 140. ([10.3847/1538-4357/aad415](https://doi.org/10.3847/1538-4357/aad415))
 17. Mihailescu T, Young PR, Brooks DH, Baker D, Green L, Long DM, van Driel-Gesztelyi L. 2025 Plasma Composition Evolution and Radiative Cooling of Flare Loops. *ApJ* - *drafted*.
 18. Barnes WT, Cargill PJ, Bradshaw SJ. 2016 Inference of Heating Properties from “Hot” Non-flaring Plasmas in Active Region Cores. I. Single Nanoflares. *ApJ* **829**, 31. ([10.3847/0004-637X/829/1/31](https://doi.org/10.3847/0004-637X/829/1/31))
 19. Barnes W, Klimchuk J, Cargill P, Bradshaw S, Reep J, Schonfeld S, Freij N, Collazzo R. 2025 ebtelplusplus: v0.4.0. ([10.5281/zenodo.15048992](https://doi.org/10.5281/zenodo.15048992))
 20. Reep JW, Unverferth J, Barnes WT, Chhabra S. 2024 Modeling Time-variable Elemental Abundances in Coronal Loop Simulations. *ApJL* **970**, L41. ([10.3847/2041-8213/ad64c3](https://doi.org/10.3847/2041-8213/ad64c3))
 21. Bradshaw SJ, Mason HE. 2003 A self-consistent treatment of radiation in coronal loop modelling. *A&A* **401**, 699–709. ([10.1051/0004-6361:20030089](https://doi.org/10.1051/0004-6361:20030089))
 22. Bradshaw SJ, Cargill PJ. 2013 The Influence of Numerical Resolution on Coronal Density in Hydrodynamic Models of Impulsive Heating. *ApJ* **770**, 12. ([10.1088/0004-637X/770/1/12](https://doi.org/10.1088/0004-637X/770/1/12))
 23. Fushimi Benavitz L, Reep JW, Tarr LA, To ASH. 2025 Spatiotemporal Low FIP Abundance: A Catalyst for Coronal Condensation. *arXiv e-prints* p. arXiv:2504.05381. ([10.48550/arXiv.2504.05381](https://doi.org/10.48550/arXiv.2504.05381))
 24. Ionson JA. 1978 Resonant absorption of Alfvénic surface waves and the heating of solar coronal loops.. *ApJ* **226**, 650–673. ([10.1086/156648](https://doi.org/10.1086/156648))
 25. Schrijver CJ. 2001 Catastrophic cooling and high-speed downflow in quiescent solar coronal loops observed with TRACE. *Sol. Phys.* **198**, 325–345. ([10.1023/A:1005211925515](https://doi.org/10.1023/A:1005211925515))
 26. de Groof A, Bastiaensen C, Müller DAN, Berghmans D, Poedts S. 2005 Detailed comparison of downflows seen both in EIT 30.4 nm and Big Bear H α movies. *A&A* **443**, 319–328. ([10.1051/0004-6361:20053129](https://doi.org/10.1051/0004-6361:20053129))
 27. Antolin P, Shibata K, Vissers G. 2010 Coronal Rain as a Marker for Coronal Heating Mechanisms. *ApJ* **716**, 154–166. ([10.1088/0004-637X/716/1/154](https://doi.org/10.1088/0004-637X/716/1/154))
 28. Antolin P, Rouppe van der Voort L. 2012 Observing the Fine Structure of Loops through High-resolution Spectroscopic Observations of Coronal Rain with the CRISP Instrument at the Swedish Solar Telescope. *ApJ* **745**, 152. ([10.1088/0004-637X/745/2/152](https://doi.org/10.1088/0004-637X/745/2/152))
 29. Kleint L, Antolin P, Tian H, Judge P, Testa P, De Pontieu B, Martínez-Sykora J, Reeves KK, Wuelser JP, McKillop S, Saar S, Carlsson M, Boerner P, Hurlburt N, Lemen J, Tarbell TD, Title A, Golub L, Hansteen V, Jaeggli S, Kankelborg C. 2014 Detection of Supersonic Downflows and Associated Heating Events in the Transition Region above Sunspots. *ApJL* **789**, L42. ([10.1088/2041-8205/789/2/L42](https://doi.org/10.1088/2041-8205/789/2/L42))
 30. Froment C, Auchère F, Bocchialini K, Buchlin E, Guennou C, Solomon J. 2015 Evidence for Evaporation-incomplete Condensation Cycles in Warm Solar Coronal Loops. *ApJ* **807**, 158. ([10.1088/0004-637X/807/2/158](https://doi.org/10.1088/0004-637X/807/2/158))
 31. Kohutova P, Verwichte E. 2016 Analysis of Coronal Rain Observed by IRIS, HINODE/SOT,

- and SDO/AIA: Transverse Oscillations, Kinematics, and Thermal Evolution. *ApJ* **827**, 39. ([10.3847/0004-637X/827/1/39](https://doi.org/10.3847/0004-637X/827/1/39))
32. Müller DAN, Hansteen VH, Peter H. 2003 Dynamics of solar coronal loops. I. Condensation in cool loops and its effect on transition region lines. *A&A* **411**, 605–613. ([10.1051/0004-6361:20031328](https://doi.org/10.1051/0004-6361:20031328))
 33. Kohutova P, Antolin P, Popovas A, Szydlarski M, Hansteen VH. 2020 Self-consistent 3D radiative magnetohydrodynamic simulations of coronal rain formation and evolution. *A&A* **639**, A20. ([10.1051/0004-6361/202037899](https://doi.org/10.1051/0004-6361/202037899))
 34. Keppens R, Zhou Y, Xia C. 2025 Modeling multiphase plasma in the corona: prominences and rain. *Living Reviews in Solar Physics* **22**, 4. ([10.1007/s41116-025-00043-2](https://doi.org/10.1007/s41116-025-00043-2))
 35. Reep JW, Antolin P, Bradshaw SJ. 2020 Electron Beams Cannot Directly Produce Coronal Rain. *ApJ* **890**, 100. ([10.3847/1538-4357/ab6bdc](https://doi.org/10.3847/1538-4357/ab6bdc))
 36. Warren HP. 2014 Measurements of Absolute Abundances in Solar Flares. *ApJL* **786**, L2. ([10.1088/2041-8205/786/1/L2](https://doi.org/10.1088/2041-8205/786/1/L2))
 37. Mondal B, Sarkar A, Vadawale SV, Mithun NPS, Janardhan P, Del Zanna G, Mason HE, Mitra-Kraev U, Narendranath S. 2021 Evolution of Elemental Abundances during B-Class Solar Flares: Soft X-Ray Spectral Measurements with Chandrayaan-2 XSM. *ApJ* **920**, 4. ([10.3847/1538-4357/ac14c1](https://doi.org/10.3847/1538-4357/ac14c1))
 38. Nordon R, Behar E. 2008 Abundance variations and first ionization potential trends during large stellar flares. *A&A* **482**, 639–651. ([10.1051/0004-6361:20078848](https://doi.org/10.1051/0004-6361:20078848))
 39. Favata F, Schmitt JHMM. 1999 Spectroscopic analysis of a super-hot giant flare observed on Algol by BeppoSAX on 30 August 1997. *A&A* **350**, 900–916. ([10.48550/arXiv.astro-ph/9909041](https://doi.org/10.48550/arXiv.astro-ph/9909041))
 40. Liefke C, Fuhrmeister B, Schmitt JHMM. 2010 Multiwavelength observations of a giant flare on CN Leonis. III. Temporal evolution of coronal properties. *A&A* **514**, A94. ([10.1051/0004-6361/201014012](https://doi.org/10.1051/0004-6361/201014012))
 41. Audard M, Güdel M, Mewe R. 2001 The XMM-Newton view of stellar coronae: Flare heating in the coronae of HR 1099. *A&A* **365**, L318–L323. ([10.1051/0004-6361:20000085](https://doi.org/10.1051/0004-6361:20000085))
 42. Kurihara M. 2025 XRISM view of a stellar flare: High-resolution Fe K spectra of HR 1099, an RS CVn-type star. *PASJ* - submitted.
 43. Seli B, Oláh K, Kriskovics L, Kővári Z, Vida K, Balázs LG, Laming JM, van Driel-Gesztelyi L, Baker D. 2022 Extending the FIP bias sample to magnetically active stars. Challenging the FIP bias paradigm. *A&A* **659**, A3. ([10.1051/0004-6361/202141493](https://doi.org/10.1051/0004-6361/202141493))
 44. Kowalski AF. 2024 Stellar flares. *Living Reviews in Solar Physics* **21**, 1. ([10.1007/s41116-024-00039-4](https://doi.org/10.1007/s41116-024-00039-4))
 45. Laming JM. 2004 A Unified Picture of the First Ionization Potential and Inverse First Ionization Potential Effects. *ApJ* **614**, 1063–1072. ([10.1086/423780](https://doi.org/10.1086/423780))
 46. Laming JM. 2015 The FIP and Inverse FIP Effects in Solar and Stellar Coronae. *Living Reviews in Solar Physics* **12**, 2. ([10.1007/lrsp-2015-2](https://doi.org/10.1007/lrsp-2015-2))
 47. Martínez-Sykora J, De Pontieu B, Hansteen VH, Testa P, Wargnier QM, Szydlarski M. 2023 The Impact of Multifluid Effects in the Solar Chromosphere on the Ponderomotive Force under SE and NEQ Ionization Conditions. *ApJ* **949**, 112. ([10.3847/1538-4357/acc465](https://doi.org/10.3847/1538-4357/acc465))
 48. Doschek GA, Warren HP. 2016 The Mysterious Case of the Solar Argon Abundance near Sunspots in Flares. *ApJ* **825**, 36. ([10.3847/0004-637X/825/1/36](https://doi.org/10.3847/0004-637X/825/1/36))
 49. Brooks DH, Baker D, van Driel-Gesztelyi L, Warren HP, Yardley SL. 2022 Detection of Stellar-like Abundance Anomalies in the Slow Solar Wind. *ApJL* **930**, L10. ([10.3847/2041-8213/ac6878](https://doi.org/10.3847/2041-8213/ac6878))
 50. Carlsson M, Leenaarts J. 2012 Approximations for radiative cooling and heating in the solar chromosphere. *A&A* **539**, A39. ([10.1051/0004-6361/201118366](https://doi.org/10.1051/0004-6361/201118366))
 51. Dere KP, Landi E, Mason HE, Monsignori Fossi BC, Young PR. 1997 CHIANTI - an atomic database for emission lines. *A&A* **125**, 149–173. ([10.1051/aas:1997368](https://doi.org/10.1051/aas:1997368))
 52. Del Zanna G, Dere KP, Young PR, Landi E. 2021 CHIANTI—An Atomic Database for Emission Lines. XVI. Version 10, Further Extensions. *ApJ* **909**, 38. ([10.3847/1538-4357/abd8ce](https://doi.org/10.3847/1538-4357/abd8ce))
 53. Asplund M, Grevesse N, Sauval AJ, Scott P. 2009 The Chemical Composition of the Sun. *ARAA* **47**, 481–522. ([10.1146/annurev.astro.46.060407.145222](https://doi.org/10.1146/annurev.astro.46.060407.145222))
 54. Mullan DJ, Mathioudakis M, Bloomfield DS, Christian DJ. 2006 A Comparative Study of Flaring Loops in Active Stars. *ApJS* **164**, 173–201. ([10.1086/502629](https://doi.org/10.1086/502629))
 55. Reep J, Brooks D. 2025 Simulation data from "Dynamic modeling of coronal abundances during flares on M-dwarf stars". ([10.5281/zenodo.17795908](https://doi.org/10.5281/zenodo.17795908))

56. Cargill PJ, Mariska JT, Antiochos SK. 1995 Cooling of Solar Flare Plasmas. I. Theoretical Considerations. *ApJ* **439**, 1034. ([10.1086/175240](https://doi.org/10.1086/175240))
57. Bradshaw SJ, Cargill PJ. 2005 The cooling of coronal plasmas. II. Properties of the radiative phase. *A&A* **437**, 311–317. ([10.1051/0004-6361:20042405](https://doi.org/10.1051/0004-6361:20042405))
58. Bradshaw SJ, Cargill PJ. 2010 The Cooling of Coronal Plasmas. III. Enthalpy Transfer as a Mechanism for Energy Loss. *ApJ* **717**, 163–174. ([10.1088/0004-637X/717/1/163](https://doi.org/10.1088/0004-637X/717/1/163))
59. Cargill PJ, Bradshaw SJ. 2013 The Cooling of Coronal Plasmas. IV. Catastrophic Cooling of Loops. *ApJ* **772**, 40. ([10.1088/0004-637X/772/1/40](https://doi.org/10.1088/0004-637X/772/1/40))
60. Reep JW, Fushimi Benavitz L, To ASH, Brooks DH, Laming JM, Antolin P, Long DM, Baker D. 2025 Radiative hydrodynamic simulations of FIP fractionation in solar flares. *arXiv e-prints* p. arXiv:2509.25695. ([10.48550/arXiv.2509.25695](https://doi.org/10.48550/arXiv.2509.25695))
61. Yang KE, Sun X, Kerr GS, Hudson HS. 2023 A Possible Mechanism for the “Late Phase” in Stellar White-light Flares. *ApJ* **959**, 54. ([10.3847/1538-4357/ad077d](https://doi.org/10.3847/1538-4357/ad077d))
62. Kurihara M, Iwakiri WB, Tsujimoto M, Ebisawa K, Toriumi S, Imada S, Tsuboi Y, Usui K, Gendreau KC, Arzoumanian Z. 2024 Investigation of Nonequilibrium Ionization Plasma during a Giant Flare of UX Arietis Triggered with MAXI and Observed with NICER. *ApJ* **965**, 135. ([10.3847/1538-4357/ad35c5](https://doi.org/10.3847/1538-4357/ad35c5))